JOURNAL OF CATALYSIS **177,** 96–104 (1998)
ARTICLE NO. CA982093

Texture and Structure of Amorphous Co-Precipitated Silica-Aluminum Phosphate Catalyst Supports

F. Wijzen,* B. Koch,† J. Rocha,‡ A. Esculcas,‡ M. Liégeois-Duyckaerts,* and A. Rulmont*,[1]

*Laboratoire de Chimie Inorganique Structurale, Département de Chimie Générale, Université de Liège, Institut de Chimie B6, B-4000 Liège, Belgium; †SOLVAY POLYOLEFINS EUROPE—BELGIUM, Rue de Ransbeek 310, B-1120 Bruxelles, Belgium; and ‡Department of Chemistry, Aveiro University, 3800 Aveiro, Portugal

Received September 23, 1997; revised March 2, 1998; accepted March 26, 1998

A series of co-precipitated silica-aluminum phosphate containing between 0 and 100 mol% silica were synthesized by a coprecipitation technique and characterized by various methods. X-ray fluorescence analysis shows that the P/Al molar ratio in the solid mixture decreases as the silica content increases, whereas this ratio remains one in the solution. Nearly all these materials are shown to be meso- and macroporous. The specific surface area decreases with increasing aluminum phosphate content, whereas the pore volume passes through a maximum at high silica content. ^{27}Al, ^{31}P, and ^{29}Si MAS-NMR spectra have also shown the existence of domains of silica and aluminum phosphate in binary supports, but these domains are not larger than a few microns, as shown by EDS measurements.

INTRODUCTION

Silica and aluminum phosphate are both used as supports in the Phillips catalysis for ethylene polymerization (1). These supports have much in common. They are isoelectronic and isostructural. However, their catalytic properties are quite different, because these two supports can exhibit different textural and surface properties. It is well known that the texture of the support, in particular its porosity, strongly influences the activity of the catalyst and also controls the polymer structure in terms of molecular weight, molecular weight distribution, and chain branching (2, 3). Support texture can be controlled by a number of parameters during this process. Moreover, the surface properties of these supports are different, the hydroxyl groups on $AlPO_4$ being more diverse (Al–OH and P–OH) and more acidic than on SiO_2.

A mixed support frequently exhibits different catalytic properties than a pure support and, therefore, leads to polymers whose mechanical properties depend upon their molecular structure (3, 4). To obtain these different catalytic properties, mechanical mixtures of the components are inefficient; intimate contact between the constituents or, even better, mixing on a molecular scale is required.

Two binary systems have been mainly studied to date, $AlPO_4$–Al_2O_3 (5–7) and SiO_2–TiO_2 (8–10). On the contrary, little is known about the SiO_2–$AlPO_4$ system. Campelo *et al.* (11) prepared different heterogeneous supports in this system by precipitating aluminum phosphate on silica. McDaniel (12) reported the preparation of a 50% SiO_2–50% $AlPO_4$ support by coprecipitation, characterized by a specific surface area of 363 m^2/g and a pore volume determined by nitrogen adsorption of 1.14 cm^3/g. After impregnation with a solution of chromium acetate in alcohol and activation, the catalyst produces polyethylene with a broad molecular weight distribution. The present paper reports the preparation and bulk characterization of various compositions of coprecipitated SiO_2–$AlPO_4$ catalyst supports which have been tested for ethylene polymerization.

METHODS

Catalyst Support Preparation

SiO_2–$AlPO_4$ catalyst supports were synthesized from tetraethylorthosilicate (TEOS), phosphoric acid, and aluminum chloride by coprecipitation with ammonia. TEOS was chosen as the silicon source to avoid alkali metals which are sometimes difficult to eliminate and could promote support-sintering during the calcination step (13). However, it is well known that TEOS is less reactive than aluminum chloride and phosphoric acid. To avoid that the aluminum phosphate precipitates before silica, TEOS has to be prehydrolyzed. In a basic medium, compact and highly cross-linked polymers are formed, while in an acidic medium, linear chains with little cross-linking are generated (14). Chain formation is a more favorable process for the final homogeneity of the supports. Walther *et al.* (15) showed that partial hydrolysis of TEOS in an acidic medium gives mixed supports in the system SiO_2–TiO_2 with a more intimate mixing than partial hydrolysis in a basic medium.

[1] To whom correspondence should be addressed. E-mail: Andre.Rulmont@ulg.ac.be.

0021-9517/98 $25.00

The amount of reagents used was calculated to obtain 0.33 mol of support. We use the notation [Si_xP_y], with x and y representing the molar percentages of silica and aluminum phosphate, respectively.

TEOS was first prehydrolyzed as follows: TEOS was mixed with ethanol ($n_{EtOH}/n_{TEOS} = 5.5$). Then, an aqueous solution of hydrochloric acid (1 mol/dm^3) and the water required for the prehydrolysis were added in order to obtain a molar ratio $r = n_{water}/n_{TEOS} = 10$ and $[H^+] = 10^{-1}$ mol/dm^3. The solution was heated for 2 h at 60°C. After this step, an aqueous solution of H_3PO_4 (85 wt%) and $AlCl_3 \cdot 6H_2O$ was added to the prehydrolyzed TEOS solution to obtain a clear acidic solution.

This acid solution was injected at the bottom of a reactor containing 500 ml of an ammonia solution, kept at 0°C and pH 8, with a pump delivering a concentrated ammonia solution (25 wt%). The precipitate was aged for 2 h at 60°C in the mother solution while being slightly stirred, then washed three times with water and three times with isopropanol, and finally dried by water exchange in isopropanol at its boiling point. During the drying process, the water-isopropanol azeotrope was first evaporated off and dried continuously on a molecular sieve (3 Å) before beeing recycled to the reactor until all water had been removed; then the dry isopropanol was evaporated off to recover a very fine free-flowing powder. The dry powder was sieved (50–200 μm) and calcined at 773 K for 4 h and then at 973 K for 2 h.

Catalyst Support Characterization

The composition of calcined catalyst supports was determined by X-ray fluorescence on a Phillips PW 1480 spectrometer.

The textural properties of the supports were determined from the nitrogen adsorption–desorption isotherms, at liquid-nitrogen boiling temperature, using a conventional volumetric method. The isotherm analysis was performed according to the method proposed by Lecloux (16). Mercury porosimetry was also carried out as a complementary method on a Carlo Erba PORO 2000 device.

^{27}Al, ^{29}Si, and ^{31}P MAS-NMR spectra were recorded on a Bruker MSL-400P spectrometer (400 MHz, 9.4T). The recording conditions are given in Table 1. Two ^{27}Al MAS-NMR techniques were also used to characterize the local environment of the aluminum nuclei. First, ^{27}Al–^{1}H cross-polarization MAS-NMR spectroscopy was used in order to prove the presence of nuclei in the vicinity of the protons. Second, the NMR central transition (CT) lines ($m = -1/2 \leftrightarrow m = +1/2$) are broadened and shifted by second-order quadrupolar interactions in the case of a quadrupolar nucleus such as ^{27}Al ($I = 5/2$); as a consequence, the spectral line is usually not very well resolved. Satellite transition ^{27}Al MAS-NMR spectroscopy (SATRAS) (17–20) can, in this case, provide better separated peaks.

TABLE 1

MAS-NMR Recording Parameters

Nucleus	MHz	Recycle delay (s)	Pulse length (μs)	MAS rate (kHz)	Reference
^{31}P	161.97	30–40	2	14–15	H_3PO_4 (85 wt%)
^{27}Al	104.26	0.5	0.6	14–15	$Al(NO_3)_3$ solution
^{29}Si	79.50	50–60	2–3	4	$(CH_3)_4Si$

Electron microscopy was performed with a Jeol SSM-840A scanning electron microscope. The powder was plated by sputtering a 20-nm thick Au–Pd layer with a Balzers SCD 030 device. For the elemental mappings we used a Link QX 2000 energy-dispersive detector (EDS) coupled with a Cambridge S360 scanning electron microscope. The powder was embedded in epoxy resin and, after cutting, the sample surface was carbon-coated before observation.

X-ray powder diffraction patterns were recorded on a Siemens D5000 X-ray diffractometer using CuKα radiation ($\lambda = 1.5406$ Å).

RESULTS

Support Composition

X-ray fluorescence data show that the molar Al/Si ratio in supports correlates well with molar Al/Si ratio in solutions. In contrast, Fig. 1 shows that the P/Al molar ratio in supports decreases when silica content increases, even though this ratio is kept equal to one in the solution. We confirmed that phosphate ions are effectively recovered in the mother solution and in the washing solutions.

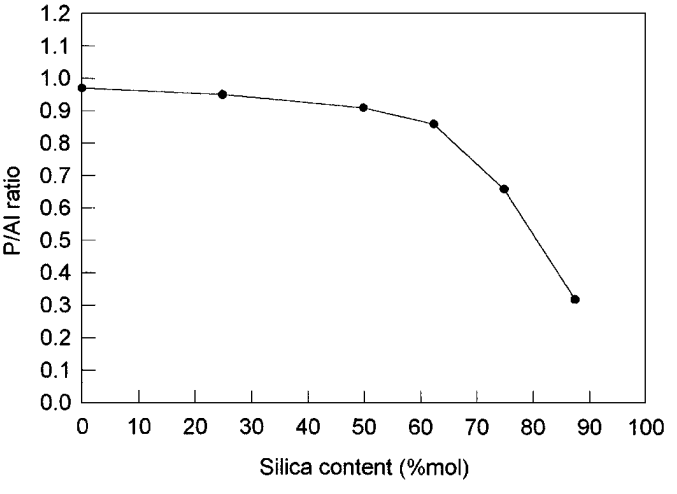

FIG. 1. Evolution of the P/Al ratio in the powder as a function of silica content in the system SiO_2–$AlPO_4$. The ratio P/Al in the solution remains stable at one.

Morphology and Texture

The morphological aspect of aluminum phosphate, silica, and sample [$Si_{50}P_{50}$] can be seen on the electron micrographs in Fig. 2. Micrograph 2A shows that aluminum phosphate consists of aggregates of small particles of relatively regular size between 100 nm and 1 μm. The structure is very open and a macroporosity, due to holes between the small particles, is clearly seen. The morphology of silica is different. Silica grains consist of tabular aggregates (Fig 2B). Micrograph 2C shows that the [$Si_{50}P_{50}$] sample consists of aggregates of small particles which create an important macroporosity, but the arrangement of the particles is less regular than in aluminum phosphate.

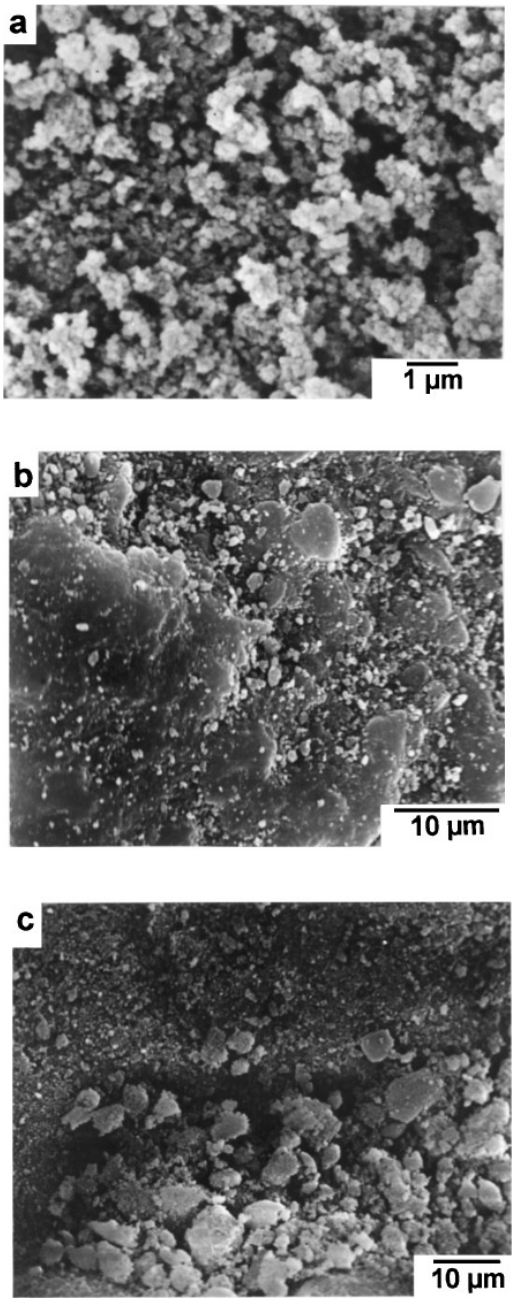

FIG. 2. Scanning electron micrographs: (a) aluminum phosphate; (b) silica; (c) [$Si_{50}P_{50}$].

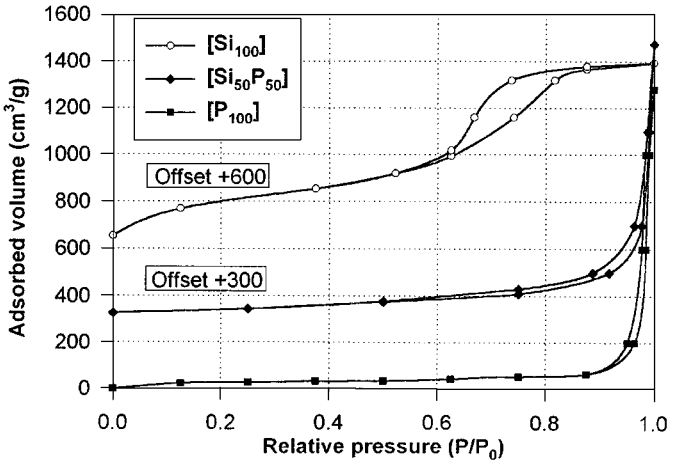

FIG. 3. Nitrogen adsorption–desorption isotherms obtained for samples [Si_{100}], [$Si_{50}P_{50}$], and [P_{100}].

The adsorption–desorption isotherms of silica, aluminum phosphate, and some binary supports are depicted in Fig. 3. According to the BDDT classification (21), the shapes of the nitrogen adsorption–desorption isotherms of the aluminum phosphate and binary supports are type II, characteristic of the presence of macropores, whereas the shape of the silica isotherm is type IV, which corresponds to the presence of mesopores. The silica isotherm hysteresis loop belongs to the de Boer classification type E ("ink-bottle" pores), while the hysteresis loop of the aluminum phosphate and binary supports is not well developed and can be classified either as type A ("cylindrical" pores) or type E ("ink-bottle" pores).

Table 2 shows that the BET surface area (S_{BET}) increases markedly with silica content. S_{BET} increases from 96 m^2/g for aluminum phosphate to 727 m^2/g for silica. Pore volume, V_P, defined as the volume of the liquid equivalent to the gas quantity adsorbed per unit of sample mass at the saturation pressure, passes through a maximum for the composition 75 SiO_2–25 $AlPO_4$.

The t-plots were constructed for each of the samples according to the Lecloux criterion (22). The t-plot of silica (Fig. 4) exhibits a marked upward deviation from the straight line, passing through the origin which is typical of capillary condensation. The t-plots of all binary supports, except for sample [$Si_{12.5}P_{87.5}$], show only a slight upward deviation, indicating the presence of a small number of mesopores, whereas t-plots of aluminum phosphate and sample [$Si_{12.5}P_{87.5}$] exhibit a slight downward deviation, followed by a slight upward deviation, indicating the presence of both micropores and mesopores. The slope of the linear part of

TABLE 2

Effect of Chemical Composition on Specific Surface Area and Porous Volume of SiO_2–$AlPO_4$ Catalyst Supports

	S_{BET} (m^2/g)	V_P (cm^3/g)	S_t (cm^3/g)	S_{cum} type A (cm^3/g)	S_{cum} type E (cm^3/g)	V_{cum} type A (cm^3/g)	V_{cum} type E (cm^3/g)	V_{Hg} (cm^3/g)
$[P_{100}]$	96	2.0	96	—	96	—	2.0	1.9
$[Si_{12.5}P_{87.5}]$	111	2.1	108	—	108	—	2.1	1.7
$[Si_{25}P_{75}]$	132	1.7	133	137	139	1.7	1.7	1.4
$[Si_{37.5}P_{62.5}]$	161	1.9	162	—	142	—	1.9	1.7
$[Si_{50}P_{50}]$	190	1.9	—	191	—	1.8	—	2.1
$[Si_{62.5}P_{37.5}]$	240	3.0	241	209	215	3.1	3.0	3.4
$[Si_{75}P_{25}]$	364	3.8	371	323	327	3.8	3.8	3.2
$[Si_{87.5}P_{12.5}]$	601	3.5	602	547	563	3.5	3.5	2.3
$[Si_{100}]$	727	1.2	732	—	700	—	1.2	0.2

Note. S_{BET}, BET specific surface area; V_P, porous volume; S_t, specific surface area obtained by the t-plot; S_{cum}, mesoporous cumulative specific surface area calculated by the Broekhoff–de Boer method with a pore model of type A or E; V_{cum} mesoporous cumulative porous volume calculated by the Broekhoff–de Boer method with a pore model of type A or E; V_{Hg}, porous volume determined by mercury penetration.

the t-plot passing through the origin is another measure of the solid specific surface area. This specific surface area, S_t, agrees very well with the corresponding S_{BET} (Table 2).

Cumulative surface area (S_{cum}) and cumulative pore volume (V_{cum}) data, obtained by the Broekhoff–de Boer method (BdB method), applied to the adsorption branch of the isotherm in the case of "ink bottle" pores (type E) and "cylindrical pores" (type A), are listed in Table 2. These data do not allow differentiating clearly between the two models. However, the agreement is slightly better in the case of the "ink bottle" shape when the silica content increases in the supports. The mixed support probably contains a distribution of pore shapes, thus preventing a simple interpretation of the adsorption curves.

The BdB method gives the distribution of surface area versus pore radius in an integral form. Some of these distributions are given in Fig. 5. Silica is essentially mesoporous and pore radii are less than 12 nm. This observation agrees well with the type IV isotherm and with the t-plot shape.

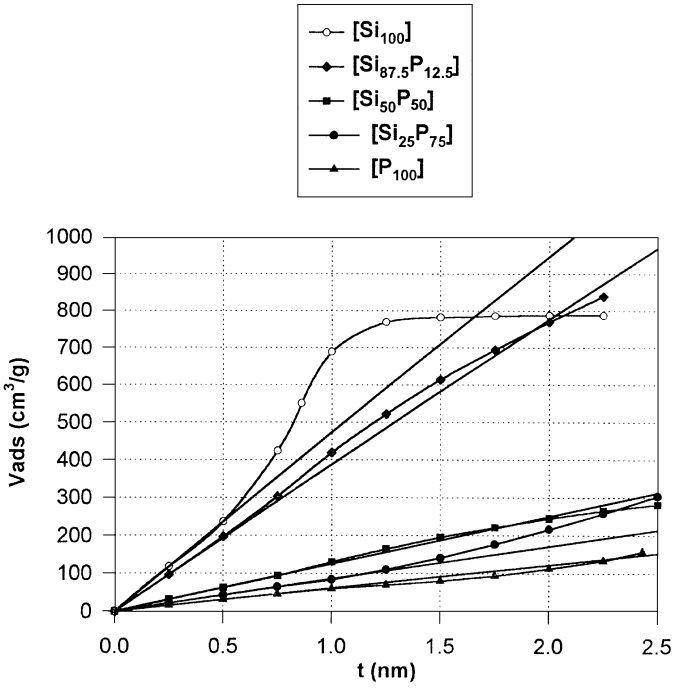

FIG. 4. t-plots: samples $[Si_{100}]$, $[Si_{87.5}P_{12.5}]$, $[Si_{50}P_{50}]$, $[Si_{25}P_{75}]$, and $[P_{100}]$.

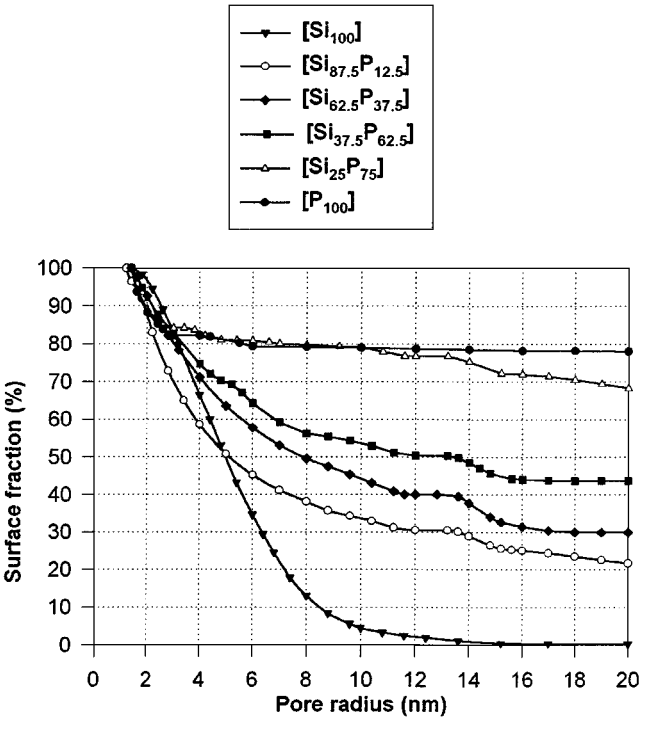

FIG. 5. Specific surface area distribution curves obtained by the BdB method on $[Si_{100}]$, $[Si_{87.5}P_{12.5}]$, $[Si_{62.5}P_{37.5}]$, $[Si_{37.5}P_{62.5}]$, $[Si_{25}P_{75}]$, and $[P_{100}]$ samples.

On the contrary, aluminum phosphate is essentially macroporous, in accordance with type II isotherm. Approximately 80% of the surface area is described by pores having a radius greater than 20 nm. In the binary system, the fraction of surface area occupied by pores whose radius is between 2 and 10 nm decreases when the aluminum phosphate content increases. These curves clearly show the presence of pores having a radius greater than 20 nm, in all binary support. These pores cannot be described by nitrogen adsorption isotherm analysis, but they can be analyzed by the mercury penetration technique.

Pore volumes obtained by mercury penetration (V_{Hg}) are given in Table 2. V_{Hg}, as a function of the chemical composition of the support, follows approximately the same trend as V_P. It goes through a maximum for $[Si_{62.5}P_{37.5}]$. Pore volumes obtained by nitrogen adsorption, V_P, are in some cases greater than pore volumes obtained by mercury penetration, V_{Hg}. These differences cannot always be explained by the fact that the pore range observable by mercury porosimetry is limited to pore radii greater than 7.5 nm. Thus, the differences observed between the two pore volume values can be explained by the inaccurate determination of the adsorbed nitrogen volume at the saturation point in the case of type II isotherms. Despite the above-mentioned inaccuracy, both techniques show a maximum pore volume for supports with a high silica content.

The distribution of pore volume versus pore size obtained by the mercury penetration technique confirms the presence of macropores in aluminum phosphate and in all binary supports. Pore size distributions are extremely large in binary supports containing more than 50 mol% of silica. These supports contain a large number of pores whose radius lies between 7.5 and 7500 nm. The presence of these pores explains the large pore volume, V_{Hg}, obtained for these supports. Pore size distribution of aluminum phosphate and binary supports containing less than 50 mol% of silica are narrower. The pore radii are mainly less than 200 nm.

X-ray Diffraction

We checked the thermal behavior with respect to crystallization up to 1573 K for all samples. All supports are amorphous after calcination at 973 K for 4 h. The crystallization of the amorphous phase can be easily detected by X ray, but the phase identification is not so obvious; the most intense peaks of the four possible crystalline phases at these temperatures (tridymite and cristobalite for SiO_2 and the corresponding phases for $AlPO_4$) are very close to each other. Furthermore, the problem of the existence of solid solutions has not yet been completely solved (23–26).

The IR absorption spectra are more sensitive to the structure type (23) and confirm the X-ray assignment. After calcination at 1373 K for 8 h, the amorphous supports, except silica, crystallize first into the tridymite phase. The presence of a tridymite phase can be confirmed by comparing the measured spectra with reference data (23, 27) and by the absence of characteristic bands of a cristobalite or phosphocristobalite phase (bands at 630, 570, 380 cm^{-1}, and the splitting of the 720 cm^{-1} band). At higher temperatures, a transition to the more stable cristobalite structure is observed for all compositions, as shown by the presence of the characteristic bands of a cristobalite or phosphocristobalite phase.

^{27}Al MAS-NMR

Results from ^{27}Al MAS-NMR are shown in Fig. 6 $AlPO_4$ spectra exhibit a peak centred at 39 ppm assigned to tetrahedral aluminum in a $Al(OP)_4$ environment (28–30). A weak peak at −10 ppm can be assigned to octahedral aluminum (28). Spectra of binary system supports are very similar to the $AlPO_4$ spectrum with an intense peak at ∼39 ppm (tetrahedral aluminum in a $Al(OP)_4$ environment) and two shoulders at 10 and −10 ppm. There is no peak in the range 55 to 70 ppm, characteristic of an $Al–(OSi)_4$ environment, nor in the range 60 to 80 ppm, corresponding to an $Al(OAl)_4$ environment (28), except for the two samples $[Si_{87.5}P_{12.5}]$ and $[Si_{75}P_{25}]$. These samples are quite different from the others. The spectra of the samples $[Si_{87.5}P_{12.5}]$ and $[Si_{75}P_{25}]$ exhibit a very broad peak from 60 to −30 ppm, extending through the spectral range of 4-, 5-, and 6-coordinated aluminum (28). This observation can be explained by phosphate deficiency in these supports. Aluminum sites are thus similar to those found in the $SiO_2–Al_2O_3$ system in which aluminum lies in 4-, 5-, and 6-coordinations (31, 32). In these

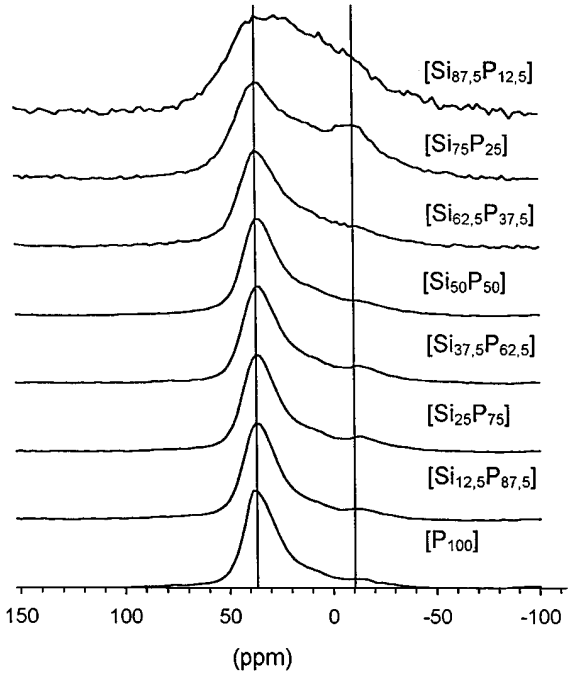

FIG. 6. ^{27}Al MAS-NMR spectra of $SiO_2–AlPO_4$ supports calcined at 973 K.

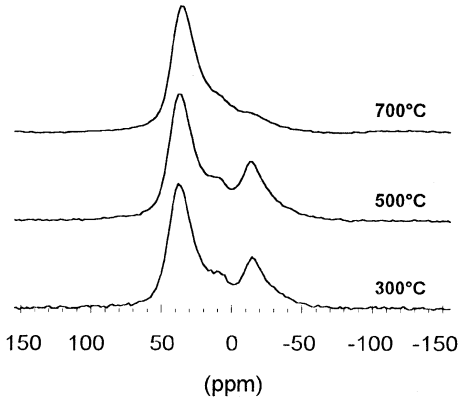

FIG. 7. ^{27}Al MAS-NMR spectra of the $[Si_{50}P_{50}]$ support calcined for 4 h at (a) 573 K, (b) 773 K, (c) 973 K.

two samples, a small part of the aluminum atoms may thus be in an $Al(OSi)_4$ or an $Al(OAl)_4$ environment.

The shoulder at −10 ppm can be assigned to octahedral aluminum surrounded by phosphorus atoms and hydroxyl groups or water molecules. Three arguments can prove this assignment. The chemical shift is close to the value observed by Blackwell (33) in $AlPO_4 \cdot 2H_2O$ for an $Al–(OP)_4(H_2O)_2$ environment (−13.2 ppm). Moreover, it has been observed on the $[Si_{50}P_{50}]$ sample that the line intensity at −10 ppm decreases with the calcination temperature (Fig. 7) which shows that this line corresponds to aluminum in an hydrated environment. Finally, ^{1}H–^{27}Al cross polarization MAS-NMR clearly shows an increase in the −10 ppm line intensity for the $[Si_{50}P_{50}]$ sample calcined at 573 K, which indicates that there are some protons around that octahedrally coordinated aluminium.

We also performed satellite transition ^{27}Al MAS-NMR spectroscopy on a second sample $[Si_{50}P_{50}]_b$ calcined at 973 K (Fig. 8). The line shape consists of a strong central transition (CT) and a series of side bands of the satellite transition (ST) ($\pm 3/2 \leftrightarrow \pm 1/2$). The side bands originating from $\pm 5/2 \leftrightarrow \pm 3/2$ transitions, could not be found because of their low intensity. The central transition (CT) consists of a main line centered at 35 ppm. The two shoulders in the spectrum of sample $[Si_{50}P_{50}]_b$ at 10 and −10 ppm are less pronounced and appear only as a broad signal. The ST side bands are symmetric (Fig. 8c). This observation suggests that there is only one aluminum type and the broad signal tails at low frequency, detected in the ^{27}Al MAS-NMR spectra of this sample, are the result of a quadrupolar effect. Moreover, we can reasonably assume that the shoulders between 20 and −10 ppm, observed in the first sample $[Si_{50}P_{50}]$ and in the other samples of the binary system, are largely produced by quadrupolar effects.

^{29}Si MAS-NMR

^{29}Si MAS-NMR spectra of silica and three binary supports are shown in Fig. 9. Silica spectra exhibit a peak at −110 ppm which can be assigned to $Si–(OSi)_4$ units (Q^4). The shoulders between −90 and −110 ppm are assigned to $Si–(OSi)_3(OH)$ and $Si–(OSi)_2(OH)_2$ units (Q^3 and Q^2 sites) (34, 35).

The binary support spectra are broader than the silica spectrum, indicating that silicon lies in a wider range of local environments. The ^{29}Si MAS-NMR spectrum is not especially influenced by the chemical composition in the binary system. The strong signal at −110 ppm is due to the presence of $Si–(OSi)_4$. The shoulders at high frequencies can be assigned to $Si(OSi)_{4-n}(OAl)_n$ units (with n = 1–3) (34) and $Si–(OSi)_3(OH)$, $Si–(OSi)_2(OH)_2$ units. The deconvolution of the total resonance line into contributions corresponding to the different silicon environments seems very difficult

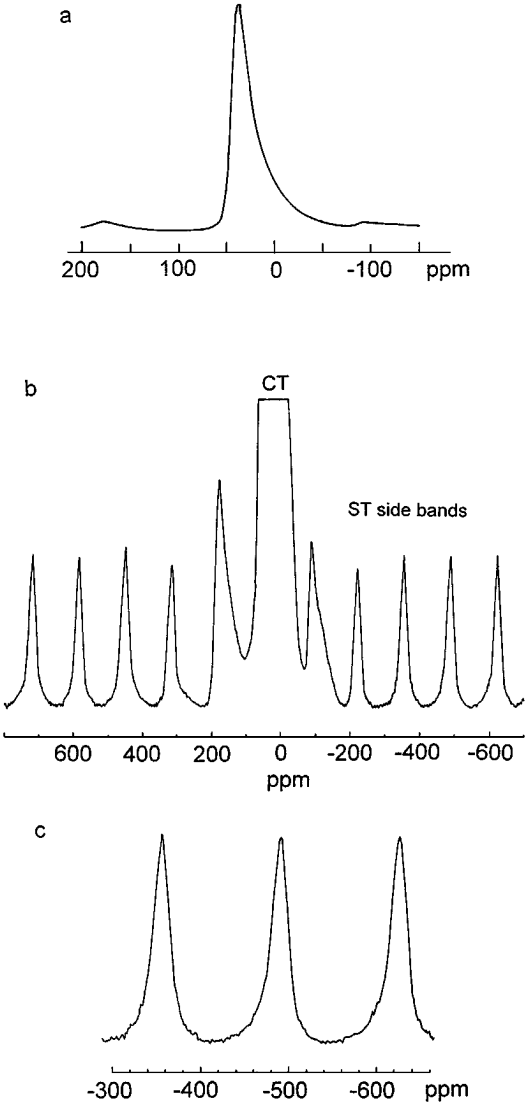

FIG. 8. ^{27}Al MAS-NMR SATRAS spectra of the $[Si_{50}P_{50}]_b$ support calcined for 4 h at 973 K : (a) ^{27}Al MAS-NMR spectra; (b) ^{27}Al MAS-NMR spectra in the range of the CT; (c) details of the $\pm 3/2 \leftrightarrow \pm 1/2$ ST side bands.

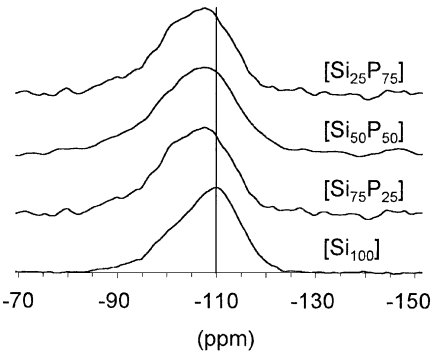

FIG. 9. ^{29}Si MAS-NMR spectra of SiO_2–$AlPO_4$ supports calcined at 973 K.

because the substitution of one Si by Al or one Si by OH gives lines lying in the same range. As intense signal is not detected from −80 to −90 ppm or at ∼120 ppm: there are only very few, if any, Si–$(OAl)_4$ and Si–$(OP)_4$ units (34, 36).

^{31}P MAS-NMR

All spectra show only one very broad ^{31}P resonance centred at −27 ppm for $AlPO_4$ and silica-aluminum phosphate. The chemical shift of peaks of binary samples is the same as the chemical shift usually observed in $AlPO_4$ (29, 37) which suggests that the environments of phosphorus nuclei are mainly $P(OAl)_4$. However, the peaks are very broad, and the chemical shift variation is only slightly influenced by the nature of the second neighbor (Si or Al) (29, 38). Thus, we cannot exclude the presence of some $P(OSi)_x(OAl)_{4-x}$ sites.

EDS

EDS results show the strong correspondence between Si, Al, and P maps. No domains of silica or aluminum phosphate greater than a few microns are detectable by this technique.

DISCUSSION

Structural Aspect

Two samples $[Si_{87.5}P_{12.5}]$ and $[Si_{75}P_{25}]$ appear to be quite different from the other mixed supports. They have a large phosphate deficiency. The ^{27}Al MAS-NMR spectra of these samples exhibit a broad feature extending from 60 to −30 ppm with a maximum of intensity at 39 ppm which can be assigned to tetrahedral aluminum in an $Al(OP)_4$ environment. For these two supports, we observed mainly $AlPO_4$ domains embedded in a silica matrix, but probably there is also some silica-alumina mixed oxide domains as shown by the width of the signal which extends through the spectral range of 4-, 5-, and 6-coordinated aluminum and, thus, covers the spectral range of $Al(OSi)_n(OAl)_{4-n}$ (with $n = 0$–4).

The ^{29}Si MAS-NMR spectra are not very sensitive to chemical composition as the signal is broad and somewhat ill-defined. However, the high intensity peak at −110 ppm, observed in all spectra, corresponds to an $Si(OSi)_4$ environment that suggests the presence of silica domains. Moreover, the low intensity of the signal from −80 to −90 ppm, or at ∼120 ppm, clearly shows that there are only very few Si–$(OAl)_4$ and Si–$(OP)_4$ units. As explained in the result section, the shoulders on the main peak can hardly give more information on the silicon environment.

The MAS-NMR spectra of ^{27}Al are much more relevant to study the sample structure. From the high intensity of the peak at 38 ppm in the ^{27}Al MAS-NMR spectra, it can be deduced that aluminum mainly lies in a Al–$(OP)_4$ environment. We can also note that aluminum atoms are not dispersed at the atomic level in the silica network because ^{27}Al MAS-NMR spectra do not contain peaks which fall in the ranges of $Al(OSi)_4$. There is also no peak in the range 60 to 80 ppm, corresponding to an $Al(OAl)_4$ environment in alumina (28). So the presence of silica-alumina domains is also unlikely (and if they are present it is only in a weak proportion) because the peak at 38 ppm is very intense and not very broad. Moreover, we have also shown in a previous work (27) that in silica-alumina catalyst support prepared with the same procedure, the ^{27}Al MAS-NMR spectra are very broad (from 80 to −30 ppm). In the silica-alumina supports the aluminum may be 4-, 5-, and 6-coordinated. Very broad ^{27}Al MAS-NMR spectra are also observed in silica-alumina gels (32) and glasses (31). So all the observations suggest the presence of small domains of aluminum phosphate and silica in the supports, but these domains are not greater than a few microns as no composition heterogeneity is detected by EDS measurements.

Three reasons can explain the formation of domains. First, the prehydrolysis conditions are too strong; the condensed species formed after prehydrolysis are, thus, too large and create some heterogeneity in the final support. Furthermore, phosphate loss has been observed in all binary supports and increases with silica content. The phosphate loss is due to the fact that the Si–O–P bond is easily hydrolyzed (39) and that phosphate ions bonded to silicon are "washed out of the support" and recovered in washing solutions. Consequently, the instability of the silicon–phosphate bonds promotes the formation of aluminum phosphate domains that are finely dispersed in the precipitate. The domains are probably linked by interface Si–O–Al bonds in accordance with the observed phosphate deficiency. That formation of small domains increases the possible number of catalytic site types, especially those located at the domain boundaries.

Charge balance when isolated aluminum or phosphate ions are introduced into the tetrahedral silica network is also unfavorable for mixing the components on a molecular scale. In the case of silica and aluminum phosphate, the

formation of small domains allows the charge compensation phenomena to be located only at domain interfaces.

The structure of silicoaluminophosphate molecular sieves (SAPO), microporous crystalline materials which contain Si, Al, P, and O atoms, has also been studied by MAS-NMR (40–44) and it is interesting to compare the MAS-NMR spectra of these materials with our results. The SAPO molecular sieves are frequently considered to be aluminophosphate frameworks with some isomorphous substitution by silicon (44). Different mechanisms can be proposed for the insertion of silicon into an $AlPO_4$ framework. The mechanism of substitution depends on the structure type, the chemical composition, and the synthesis conditions of the SAPOs. The substitution can involve replacement of one phosphorus by one silicon which gives an intense ^{29}Si MAS-NMR signal around −92 ppm, corresponding to a $Si(OAl)_4$ environment (40–44). This substitution is not observed in our supports. In SAPOs, the substitution can also occur in a heterogeneous way by replacing systematically all Al and P atoms by Si atoms in some region of the crystal, starting from the external surface. These Si domains give a signal around −110 ppm (43, 44). Some aluminum atoms can also be incorporated in these Si domains to create aluminosilicate (SA) domains next to silicoaluminophosphate (SAPO) domains with an $Al(OSi)_4$ environment. In the two-dimensional representation of substitution in SAPO developed by Martens (44), the two crystal domains are linked by Si–O–Al bonds.

Textural Aspect

Textural properties are very sensitive to the chemical composition of the support. The specific surface area decreases as the aluminum phosphate content increases, whereas pore volume passes through a maximum for a support with a high silica content. This evolution shows that the texture of mixed supports is very different from a mechanical mixture of silica and aluminum phosphate.

Two compositions, $[Si_{87.5}P_{12.5}]$ and $[Si_{75}P_{25}]$, are characterized by a large specific surface area and pore volume. These supports have a high mesoporosity, resulting in a large specific surface area, as well as a high macroporosity which is responsible for the widespread porosity. Macroporosity is closely related to the drying method.

CONCLUSION

Silica-aluminum phosphate porous supports, containing between 0 and 100 mol% of silica, were synthesized by a coprecipitation technique. Textural analysis proved the strong influence of the chemical composition of the support on its textural properties. The specific surface area decreases as the aluminum phosphate content increases, whereas pore volume passes through a maximum for a support with a high silica content.

Evidence of the presence of small domains of aluminum phosphate and silica in the binary support was obtained from ^{27}Al MAS-NMR spectra. ^{29}Si MAS-NMR spectra are less useful for that purpose. These domains are not greater than a few microns, as shown by the EDS measurements. The domain boundaries can act as sites of particular catalytic activity.

ACKNOWLEDGMENTS

The authors thank SOLVAY Polyolefins Europe-Belgium for financial support and Dr. M. Köhler for performing the adsorption–desorption of nitrogen, the mercury penetration analysis, and for helpful discussions.

REFERENCES

1. McDaniel, M. P., and Johnson, M. M., *J. Catal.* **101**, 446 (1986).
2. Marsden, C. E., *in* "Studies in Surface Science and Catalysis" (G. Poncelet, P. A. Jacobs, P. Grange, and B. Delmon, Eds.), Vol. 63, p. 215. Elsevier, Amsterdam, 1991.
3. McDaniel, M. P., *Ind. Eng. Chem. Res.* **27**, 1559 (1988).
4. McDaniel, M. P., and Johnson, M. M., *Macromolecules* **20**, 773 (1987).
5. Cheung, T. T. P., Willcox, K. W., McDaniel, M. P., Johnson, M. M., Bronnimann, C., and Frye, J., *J. Catal.* **102**, 10 (1986).
6. Hill, R. W., Kehl, W. L., and Lynch, T. J., U.S. Patent 4,219,444 (1980).
7. McDaniel, M. P., and Johnson, M. M., U.K. Patent 2,090,238A (1981).
8. McDaniel, M. P., Welch, M. B., and Dreiling, M. J., *J. Catal.* **82**, 118 (1983).
9. Conway, S. J., Falconer, J. W., Rochester, C. H., and Downs, G. W., *J. Chem. Soc. Faraday Trans. 1* **85**, 1841 (1989).
10. Dietz, R. E., U.S. Patent 3,887,494 (1975).
11. Campelo, J. M., Garcia, A., Luna, D., and Marinas, J. M., *Can. J. Chem.* **62**, 638 (1984).
12. McDaniel, M. P., U.K. Patent 2,090,158 (1981).
13. Uytterhoeven, J., André, J., and Fripiat, J. J., *Bull. Soc. Chim. Fr.*, 1804 (1965).
14. Brinker, C. J., Keefer, K. D., Schaefer, D. W., Assink, R. A., Kay, B. D., and Ashley, C. S., *J. Non-Cryst. Solids* **63**, 45 (1984).
15. Walther, K. L., Wokaun, A., Handy, B. E., and Baiker, A., *J. Non-Cryst. Solids* **134**, 47 (1991).
16. Lecloux, A. J., *in* "Catalysis Sciences and Technology" (J. R. Anderson and M. Boudart, Eds.), Vol. 2, p. 171. Springer-Verlag, Berlin, 1981.
17. Samoson, A., *Chem. Phy. Lett.* **119**, 29 (1985).
18. Jäger, C., *J. Magn. Res.* **99**, 353 (1992).
19. Rocha, J., and Pedrosa de Jesus, J. D., *Clay Miner.* **29**, 287 (1994).
20. Jäger, C., Rocha, J., and Klinowski, J., *Chem. Phys. Lett.* **188**, 208 (1992).
21. Brunauer, S., Emmet, P. H., and Teller, E., *J. Am. Chem. Soc.* **62**, 309 (1938).
22. Lecloux, A. J., and Pirard, J. P., *J. Colloid Interface Sci.* **70**, 265 (1979).
23. Rey, T., *Z. Kristallogr.* **123**, 263 (1966).
24. Robinson, P., and McCartney, E. R., *J. Am. Ceram. Soc.* **47**, 587 (1964).
25. Kobayashi, T. J., *Ceram. Assoc.* **72**, 94 (1964).
26. Horn, W. F., and Hummel, F. A. *Glass Ceram. Res. Bull.* **26**, 47 (1979).
27. Wijzen, F., Ph.D. thesis, University of Liège, 1996.
28. Bradley, S. M., Howe, R. F., and Kydd, R. A., *Magn. Reson. Chem.* **31**, 883 (1993).
29. Sanz, J., Campelo, J. M., and Marinas, J. M., *J. Catal.* **130**, 642 (1991).
30. Coury, L., Babonneau, F., Henry, and Livage, M. J., *C.R. Acad. Sci. Paris* **309**, 799 (1989).
31. Risbut, S. H., Kirkpatrick, R. J., Taglialavore, A. P., and Montez, B., *J. Am. Ceram. Soc.* **70**, c-10 (1987).

32. Selvaraj, U., Komarneni, S., and Roy, R., *J. Solid State Chem*. **106**, 73 (1993).
33. Blackwell, C. S., and Patton, R. L., *J. Phys. Chem*. **88**, 6135 (1984).
34. Thomas, J. M., and Klinowski, J., *Adv. Catal.* **33**, 199 (1985).
35. Maciel, G. E., and Sindorf, D. W., *J. Am. Chem. Soc.* **102**, 7606 (1980).
36. Szu, S. P., Klein, L. C., and Greenblatt, M., *J. Non-Cryst. Solids.* **143**, 121 (1992).
37. Brow, R. K., Kirkpatrick, R. J., and Turner, G. L., *J. Am. Ceram. Soc.* **73**, 2293 (1990).
38. Tian, F., Pan, L., Wu, X., and Wu, F., *J. Non-Cryst. Solids.* **104**, 129 (1988).
39. Iler, R. K., *in* "The Chemistry of Silica," p. 190. Wiley-Interscience, New York, 1979.
40. Blackwell, C. S., and Patton, R. L., *J. Phys. Chem*. **92**, 3965 (1988).
41. Freude, D., Ernst, H., Hunger, M., Pfeifer, H., and Jahn, E., *Chem. Phys. Lett.* **143**, 477 (1988).
42. Ojo, A. F., Dwyer, J., Dewing, J., O'Malley, P. J., and Nabhan, A., *J. Chem. Soc. Faraday Trans.* **88**, 105 (1992).
43. Martens, J. A., Grobet, P. J., and Jacobs, P. A., *J. Catal.* **126**, 299 (1990).
44. Martens, J. A., and Jacobs, P. A., *in* "Studies in Surface Science and Catalysis" (J. C. Janssen, M. Stöcker, H. G. Karge, and J. Weitkamp, Eds.), Vol. 85, p. 653. Elsevier, Amsterdam, 1994.